Research Article

Antimicrobial Electrodeposited Silver-Containing Calcium Phosphate Coatings

T. Mokabber, H. T. Cao, N. Norouzi, P. van Rijn,* and Y. T. Pei

Cite This: *ACS Appl. Mater. Interfaces* 2020, 12, 5531−5541

Read Online

ACCESS | Metrics & More | Article Recommendations | Supporting Information

ABSTRACT: Biocompatible antimicrobial coatings may enhance the function of many orthopedic implants by combating infection. Hydroxyapatite is a choice mineral for such a coating as it is native to bone and silver would be a possible antimicrobial agent as it is also commonly used in biomedical applications. The aim of the research is to develop a silver-containing calcium phosphate (Ag/Ca-P) coating via electrochemical deposition on titanium substrates as this allows for controlled coating buildup on complex shapes and porous surfaces. Two different deposition approaches are explored: one-step Ag/Ca-P(1) deposition coatings, containing silver ions as microsized silver phosphate particles embedded in the Ca-P matrix; and via a two-step method (Ag/Ca-P(2)) where silver is deposited as metallic silver nanoparticle on the Ca-P coating. The Ag/Ca-P(1) coating displays a bacterial reduction of 76.1 ± 8.3% via Ag-ion leaching. The Ag/Ca-P(2) coating displays a bacterial reduction of 83.7 ± 4.5% via contact killing. Interestingly, by preincubation in phosphate-buffered saline solution, bacterial reduction improves to 97.6 ± 2.7 and 99.7 ± 0.4% for Ag/Ca-P(1) and Ag/Ca-P(2) coatings, respectively, due to leaching of formed $AgCl_x^{(x-1)-}$ species. The biocompatibility evaluation indicates that the Ag/Ca-P(1) coating is cytotoxic towards osteoblasts while the Ag/Ca-P(2) coating shows excellent compatibility. The electrochemical deposition of highly bactericidal coatings with excellent biocompatibility will enable us to coat future bone implants even with complex or porous structures.

KEYWORDS: hydroxyapatite, electrochemical deposition, silver nanoparticles, antimicrobial, biocompatibility
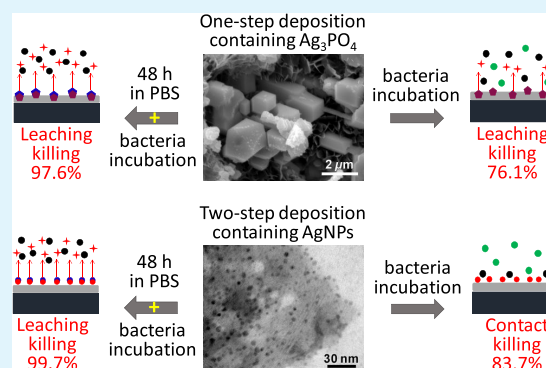
1. INTRODUCTION

The function of a biomedical implant inside the human body is determined by its physical performance as well as the biological interaction. It is well-known that chemical, physical, and mechanical properties of the implant for a large part dictate the interaction with the human body in terms of biocompatibility and bioactivity.[1−3] However, in addition to the interaction with tissue cells, also interaction with other cells such as bacteria is often encountered giving rise to a biomaterial (implant) associated infection.[4,5] Therefore, the next generation of metallic implants not only needs to fulfill the biocompatibility and bioactivity but also needs to prevent infection.[6−8] Our earlier work on the improvement of titanium (Ti) implants has shown that synthesizing a smooth layer of calcium phosphate coating on Ti surface via electrochemical deposition, influences the cell adhesion and viability, and subsequently implant biocompatibility.[9] However, calcium phosphate coatings are susceptible to bacterial infections caused by the adhesion and colonization of bacteria on the implant surface. Biomaterial-associated infections, particularly in the bone due to hampered vascularization, are difficult to treat because the bacteria establish mature biofilms and develop resistance to antibiotic treatments.[10−12] Therefore, for an infected implant, the

removal and replacement is often needed and inflicts substantial burden on the patient.[13,14]

To prevent the initial implant-associated infection, several surface antimicrobial strategies have been proposed.[15,16] One of these approaches is silver-containing hydroxyapatite (HA) coating to provide antimicrobial activity while maintaining the bioactivity of the implant. Silver (Ag) is a well-known antimicrobial agent and effective against a broad spectrum of bacterial strains (more than 650 pathogens) while being relatively low toxic to mammalian cells. Ag ions, compounds, and nanoparticles (NPs) are increasingly used for infection treatment due to their excellent antimicrobial properties. Regarding the antimicrobial properties, the results of previous studies are promising because silver-containing hydroxyapatite structures improve the bactericide effect.[17−20] Shi et al.[17] prepared silver-doped hydroxyapatite nanocrystals using the hydrothermal method with the silver concentration of 0.04–

197 ppm, which revealed 97% bacteria reduction for the highest silver concentration. Xie et al.[19] electrochemically deposited hydroxyapatite coatings containing silver nanoparticles, which were supported using Ag-ion coordinating polymer chitosan, exhibited high antimicrobial properties against *Staphylococcus epidermidis* and *Escherichia coli*. The mechanism was shown to be a releasing system and a dual function of chitosan and silver led to a 94% killing efficiency.

The comparative role of silver nanoparticles (AgNPs) and silver ions (Ag^+) in the antimicrobial activity and toxicity against mammalian cells is still a matter of discussion.[12,21,22] Moreover, the antimicrobial mechanism of silver-containing materials is not fully understood yet. Contact killing and leaching killing are two mechanisms that have been proposed. Bacteria may be killed by direct contact with metallic AgNPs, which can attach to the cell wall of the bacteria, form pits in the cell membrane, penetrate the cytoplasm, and eventually cause cell death.[23−25] Another possibility is the gradual release of Ag^+ ions from silver-containing material, followed by their interaction with thiol groups in proteins, inhibition on cell respiration and DNA replication.[14,17] On the other hand, Cao et al.[26] have reported that the antimicrobial activity of AgNPs is the result of the microgalvanic effect between the AgNPs and Ti matrix and independent of the toxicity of silver ions. Therefore, there is remarkable variation in the observed antimicrobial mechanism of silver-containing materials. The relationship between antimicrobial activity and the type of silver in the silver-containing materials is not clearly understood. Hence, it is crucial to characterize the chemical composition of the materials thoroughly and identify the coating behavior under appropriate working conditions to elucidate why the coating is a success. Determining the role of silver type in the antimicrobial properties and biocompatibility of silver-containing coatings has outstanding importance, which can provide a great opportunity to improve the bactericidal coatings for future biomedical implants.

The aim of the research is to synthesize silver-containing calcium phosphate coatings that display high antimicrobial effectiveness. Two approaches are used, ionic silver and silver nanoparticle-containing coatings to identify their role in the antimicrobial properties and biocompatibility. To deposit silver-containing calcium phosphate coatings, either with silver ions or silver nanoparticles, the electrochemical deposition is applied, which allows the formation of a uniform coating on highly irregularly shaped objects.[27] The chemical composition and microstructure of the coatings are characterized. Furthermore, *Staphylococcus aureus* and osteosarcoma cells (SaOs) are used to evaluate the antimicrobial properties and biocompatibility of the coatings, respectively. The influence of preincubation in different solutions on the antimicrobial properties of the coatings is studied and the overall antimicrobial mechanism of the coatings is investigated.

2. MATERIALS AND METHODS

2.1. Synthesis and Characterization of Ag/Ca-P Coatings. *2.1.1. Electrodeposition of Ag/Ca-P Coatings.* The Ag/Ca-P coating containing ionic silver is deposited through electrochemical deposition on Ti substrates through one step and is depicted as Ag/Ca-P(1). The details of deposition and substrate preparation are based on a previously established method by us.[9] An electrolyte solution containing 0.042 M $Ca(NO_3)_2 \cdot 4H_2O$ (Alfa Aeser), 0.025 M $NH_4H_2PO_4$ (Alfa Aeser), 10 mM $AgNO_3$ (Sigma-Aldrich), and 1.5 wt % of H_2O_2 is prepared in distilled water. Pulsed electrodeposition is conducted in a regular two-electrode cell and carried out with fixed

frequency (1 Hz) in potentiostat mode at −1.4 V cathodic potential at 65 ± 1 °C. The deposition of Ag/Ca-P coating containing AgNPs is conducted through two separate steps: first Ca-P coating is deposited on the Ti substrate for 1 min following the same protocol as reported previously.[9] In the second step, AgNPs are deposited onto the Ca-P coating, which is discussed in more detail in ref 28. The deposition of AgNPs is also conducted in a conventional two-electrode cell in which the Ca-P coating is used as the cathode, and a platinum sheet is used as the anode. The electrolyte solution, which contains 1.25 mM NaCl (Merck), is heated to 95 ± 1 °C. Afterward, 1.25 mM $AgNO_3$ (Sigma-Aldrich) is added to the electrolyte under stirring. The electrochemical deposition of AgNPs is conducted at a constant voltage of −1.4 V for 6 min, and Ag^+ is reduced to Ag^0 at the surface of the Ca-P coating. The coating deposited in two steps is depicted as Ag/Ca-P(2).

2.1.2. Characterization of Ag/Ca-P Coatings. The phase composition of the coatings is studied by X-ray diffraction (XRD, Bruker D-8 Advance-Germany Spectrometer), with Cu Kα radiation of λ = 1.5406 Å under 40 kV and 40 mA. XRD data are collected in the 2θ range of 10−70° with a step size of 0.02°. The surface morphology of the coatings is observed by using a Philips ESEM-XL30 environmental scanning electron microscope (ESEM). The element distribution of the Ag/Ca-P(1) coating is further studied by SEM equipped with energy-dispersive spectroscopy (SEM/EDS). Before SEM observation, the coatings are sputtered with gold. X-ray photoelectron spectroscopy (XPS) is employed to investigate the elemental compositions and chemical bonding of the Ag/Ca-P(1) coating using a Surface Science SSX-100 electron spectroscopy for chemical analysis (ESCA) instrument with a monochromatic Al Kα X-ray source ($h\nu$ = 1486.6 eV). During data acquisition, the pressure in the measurement chamber is kept below 2×10^{-7} Pa. Spectra analysis includes a Shirley background subtraction and peak separation adopting mixed Gaussian−Lorentzian functions in a least-squares curve fitting program (Winspec, developed at the LISE laboratory of the Faculte's Universitaires Notre-Dame de la Paix, Namur, Belgium). The microstructure of the Ag/Ca-P(2) coating is revealed by transmission electron microscope (TEM, JEOL 2010F, 200 kV).

2.2. Silver Ion Release. The study of silver ion release is carried out by immersing the substrate bearing the Ag/Ca-P coating in 10 mL phosphate-buffered saline (PBS) solution and incubating at 37 °C with a shaking speed of 50 rpm in the dark. Experiments for all conditions were separately analyzed in triplicate. The release rate is determined by extracting 1 mL Ag released solution after 6, 12, 24, 48, and 72 h and analyzed by inductively coupled plasma optical emission spectrometer (ICP-OES) OPTIMA 7000 DV (PerkinElmer). The same volume of fresh PBS is added to the samples to keep a constant incubation volume.

2.3. Antimicrobial Activity. *2.3.1. Bacteria Strain and Growth Condition.* Gram-positive *S. aureus* (ATCC 12600) is used in this study. The bacteria strain is first grown overnight at 37 °C on a blood agar plate from a frozen stock solution [dimethyl sulfoxide (DMSO)]. One colony is inoculated in 10 mL tryptone soya broth (TSB; Oxoid, Basingstoke, U.K.) and incubated at 37 °C for 24 h. This preculture is used to inoculate the main culture of 200 mL TSB that is allowed to grow for 16 h at 37 °C. The bacteria from the main culture are harvested by centrifugation at 6500*g* for 5 min at 10 °C for three times and washed with PBS solution. Subsequently, bacteria are sonicated on the ice at 30 W for 30 s (Vibra Cell model VCX130; Sonics and Materials Inc., Newtown, CT) to break down the bacterial clusters. Afterward, the number of bacteria in suspension is determined by the Bürker-Türk counting chamber, and the concentration is adjusted to 1.0×10^5 CFU/mL (colony forming units) for further experiments.

2.3.2. Colony Count Method. The colony count method is an appropriate way to quantitatively evaluate the bacteria-colony reduction on the coatings. All the laboratory supplies, as well as the coatings, are sterilized at 121 °C for 20 min by autoclave. Before introducing the bacteria suspension, the coatings are pretreated by PBS, ultrapure water, and culture medium without bacteria. To

pretreated the coatings by mentioned solutions, the coatings are immersed in 500 μL of the solution inside 24-well plates, and incubated at 37 °C with a shaking speed of 50 rpm in the dark for 48 h. Subsequently, the solutions are extracted, and 1 mL of bacteria suspension with an initial concentration of 1.0×10^5 CFU/mL is introduced onto the coatings, both treated and nontreated, and followed by incubation at 37 °C for 24 h. After incubation, the coatings are rinsed with PBS to remove the poorly attached bacteria. To detach the biofilm formed on the coatings, the coatings are sonicated using an ultrasonic bath for 5 min in 1 mL PBS. For subsequent bacterial counting, the detached bacteria suspension is serially diluted in 10-fold steps with PBS. The diluted suspension is spread over a TSB agar plate and incubated at 37 °C overnight; the active bacteria are counted and used to calculate the bacteria reduction percentage ($R\%$) according to the following formula

$$R = \frac{N_c - N_s}{N_s} \times 100\%$$

where N_c is the number of bacteria on the pure Ca-P coating as the control and N_s is the number of bacteria on the Ag/Ca-P coatings. All the experiments are performed in triplicate.

2.3.3. Live/Dead Staining. To study the initial bacterial adhesion, bacteria that are seeded on the coatings for 4, 6, and 24 h are stained with a Live/Dead BacLight kit (Invitrogen). After each time point, the culture medium is removed, and the samples are rinsed with PBS. The live/dead staining solution is prepared by mixing components A (SYTO 9) and B (propidium Iodide) with 1:1 ratio. After adding the staining solution, samples are incubated for 15 min at room temperature in the dark. The cells are imaged by fluorescence microscope (Leica DFC350 FX).

2.4. Biocompatibility. *2.4.1. 2,3-Bis(2-methoxy-4-nitro-5-sulfophenyl)-2H-tetrazolium-5-carboxanilide (XTT) Assay.* Osteosarcoma cells (SaOs), a human osteoblast cell line, with a concentration of 4.0×10^4 cells/mL, are used to evaluate the biocompatibility of Ag/Ca-P coatings. The metabolic activity of the cells is studied by 2,3-bis(2-methoxy-4-nitro-5-sulfophenyl)-2H-tetrazolium-5-carboxanilide (XTT) assay (AppliChem A8088). After 24 h of culture, samples are rinsed with PBS, and fresh medium along with 250 μL of XTT reaction mixture is added to each well. After adding the mixture, samples are incubated for 3 h at 37 °C in an atmosphere of 5% CO_2. Afterward, 200 μL of the solution from each well is transferred to a 96-well plate. The absorbance is recorded at 485 and 690 nm by a FLUOStar OPTIMAL microplate reader (BMG LABTECH). Experiments are performed in triplicate.

2.4.2. Live/Dead Staining. To determine the viable cells on the Ag/Ca-P coatings, the cells that are cultured for 24 h are stained with a Live/Dead BacLight kit following the same protocol that is described in Section 2.3.3.

2.4.3. Cell Fixation and Sample Preparation for Cell Imaging. To study cell adhesion and spreading, after 24 h of culture, the cells are fixed with 3.7% paraformaldehyde (PFA, Sigma-Aldrich) at room temperature for 20 min. Before SEM observation, the samples are dehydrated in a graded ethanol series (25, 50, 75, 98, and 100 vol %) followed by washing with hexamethyldisilazane (HMDS). Finally, the samples are sputtered with gold.

2.5. Statistical Analysis. All data points are expressed as mean values ± standard deviations with $n = 3$. Statistical analysis is performed using Origin 8.0 software by one-way analysis of variance (ANOVA), followed by Tukey's test. Statistical significance is considered at a value of $p < 0.05$.

3. RESULTS AND DISCUSSION

3.1. Characterization of Ag/Ca-P Coatings. The XRD patterns of Ca-P and Ag/Ca-P coatings after depositing on Ti substrates are illustrated in Figure 1. As it is expected, the XRD pattern of the Ca-P coating shows the typical peaks of hydroxyapatite (HA), octacalcium phosphate (OCP), and Ti.[29] The XRD pattern of the Ag/Ca-P(2) coating shows the
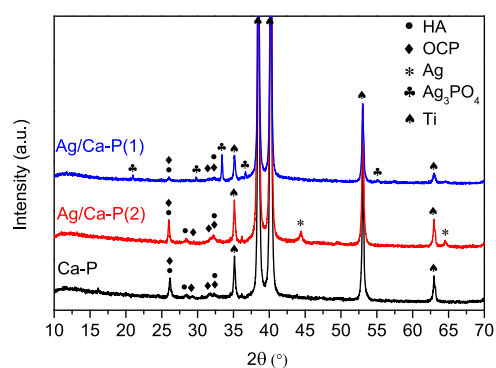

Figure 1. X-ray diffraction patterns of Ca-P and Ag/Ca-P coatings.

same peaks as well as the diffraction peaks of pure silver. The main peak of metallic silver at 2θ value of 38.1° has an overlap with the diffraction peak of titanium. However, the diffraction peaks at 2θ values of 44.3 and 64.4° are corresponding to metallic silver (JCPDS No. 04-0783). In the XRD pattern of the Ag/Ca-P(1) coating, no diffraction peak related to metallic silver is observed, but well-distinguished diffraction peaks of silver phosphate at 2θ values of 20.9, 29.7, 33.4, and 36.8° can be seen (JCPDS No. 06-0505). For Ag_3PO_4 of body-centered cubic structure, the XRD peak intensity ratio of (200) to (110) planes, which correspond to the peaks at 2θ values of 29.7 and 20.9° is 1.29. In the XRD pattern of Ag/Ca-P(1) coating, this ratio is 0.83 indicating that the structure of deposited Ag_3PO_4 crystals is primarily composed of {110} crystal facets and the crystallographic structure is rhombic dodecahedral.[30,31]

The SEM observation reveals that the morphology of Ag/Ca-P(1) coating consists of microsized particles embedded in a flat and smooth layer (Figure 2a). The high magnification SEM images in Figure 2b,c show that the particles are rhombic dodecahedral crystals consisting of 12 well-defined crystal faces, which are enclosed by {110} facets.[30,32] According to the EDS elemental analysis in Figure 2, the deposited background layer is a Ca-P layer because of the existence of Ca, P, and O ions. Meanwhile, the presence of Ag and P ions and the absence of Ca ions in the particles demonstrate that the embedded particles are Ag_3PO_4 crystals. These findings agree well with the XRD results.

Furthermore, XPS spectroscopy is used to determine the surface composition and the chemical state of the silver in the Ag/Ca-P(1) coating. Figure 3 illustrates the XPS wide scan spectra conducted on the surface of Ag/Ca-P(1) coating and also the XPS high-resolution scan spectra of the Ag element. The presence of C 1s peak is attributed to the adsorption of impurity hydrocarbons. This peak is used for calibrating the binding energy (BE) to correct sample charging (BE of C 1s = 284.8 eV).[33] In the XPS wide scan spectra (Figure 3a), the peaks corresponding to Ca 2p, P 2p, O 1s, and Ag 3d are distinct and in good agreement with those reported in literature.[34,35] The XPS high-resolution spectrum of Ag 3d is shown in Figure 3b. As it is seen, the Ag 3d spectrum consists of two individual peaks, which can be attributed to Ag ($3d_{5/2}$) at BE of 367.8 eV and Ag ($3d_{3/2}$) at BE of 373.7 eV, respectively, and the slitting of the 3d doublet is 5.9 eV. The Ag 3d high-resolution spectrum can be further deconvoluted in three different peaks originating from metallic (Ag, 368.6 eV) and oxide states (Ag_2O, 368.2 eV and AgO, 367.8 eV).[36] The deconvolution analysis demonstrates that about 38 and 50% of the silver is respectively in Ag^+ and Ag^{2+} chemical state;
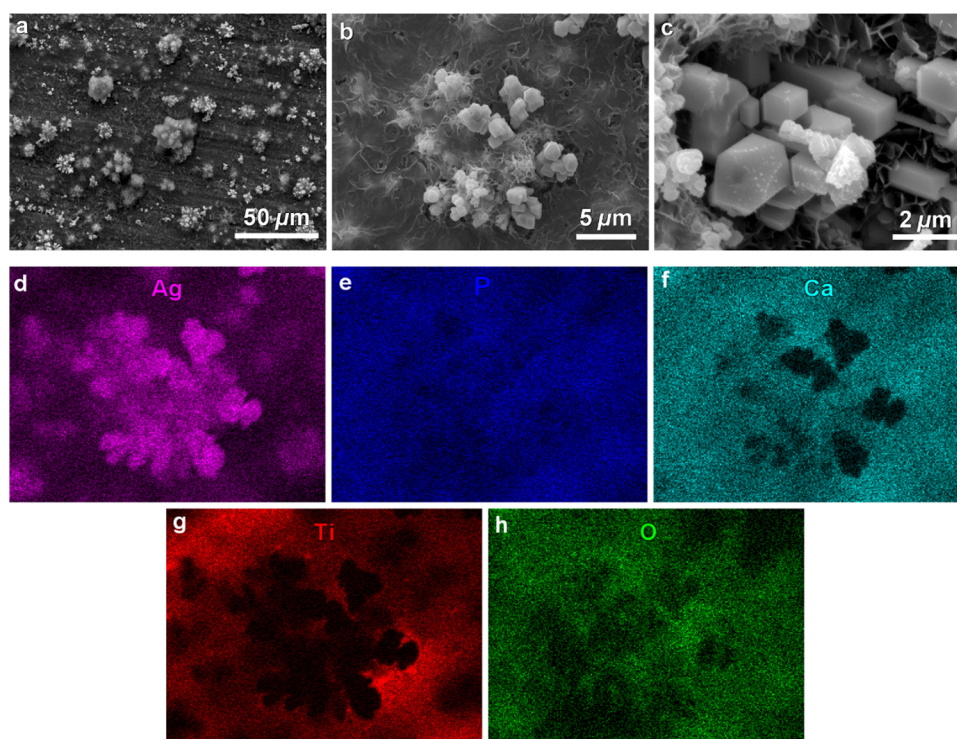
Figure 2. (a−c) SEM micrograph at different magnifications showing the size distribution and morphology of Ag_3PO_4 particles in the Ag/Ca-P(1) coating, (d−h) EDS elemental mappings corresponding to the SEM micrograph in (b).
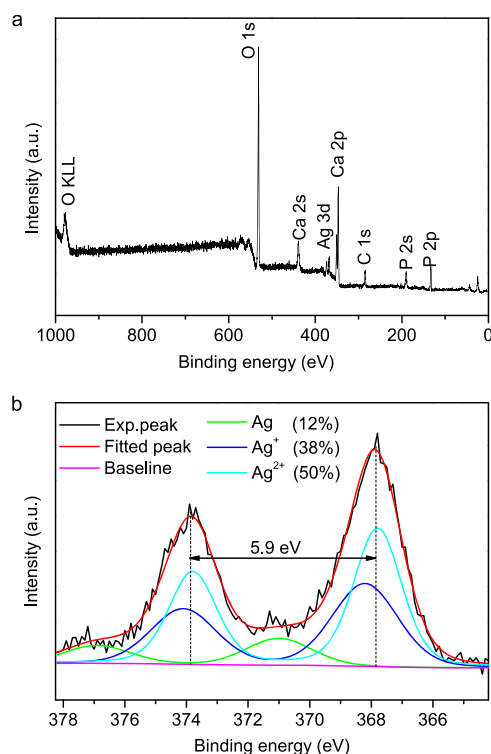

Figure 3. XPS survey spectra of the Ag/Ca-P(1) coating (a) and high-resolution scan of Ag (3d) spectra (b).

nonetheless, about 12% of the silver is in Ag^0 state. Consequently, most of the silver in the Ag/Ca-P(1) coating is in the ionic state rather than a metallic state. The XPS results provide additional evidence for the formation of Ag_3PO_4 in the Ag/Ca-P(1) coating.

By the combination of XRD, EDS, and XPS analyses, it can be concluded that in the electrochemical deposition process of the Ag/Ca-P(1) coating, Ag^+ ions prefer to react with PO_4^{3+} ions and form Ag_3PO_4 particles rather than to dope inside the structure of Ca-P crystals. This finding is in contrast with the previous studies, which reported that silver ions could be doped inside the structure of the Ca-P crystals during the electrodeposition process.[37] During the electrodeposition of the Ag/Ca-P(1) coating, silver ions have a stronger tendency to react with PO_4^{3+} ions rather than to replace the Ca ions. This can be attributed to the larger ionic radius of silver compared to calcium (r_{Ag+} = 1.28 Å and r_{Ca2+} = 0.99 Å) and also to the higher reaction intensity of phosphate ions with silver.[38,39] Rameshbabu et al. synthesized silver-substituted nanosized hydroxyapatite ($Ca_{10-x}Ag_x(PO_4)_6(OH)_2$) via microwave processing.[38] They reported that in a higher concentration of silver ($x > 0.4$), the silver phosphate crystals are formed. They claimed that the silver ions size effect, polarizability, charge, chemical nature of silver, and crystal size of the HA might reduce the substitution of calcium ions by silver ions.

The microstructure of the Ag/Ca-P(2) coating is examined by SEM and TEM (Figure 4). As it is seen in Figure 4a, the Ag/Ca-P(2) coating has a similar morphology to the Ca-P coating synthesized under similar conditions in our previous study. The surface morphology of Ag/Ca-P(2) coating is smooth with low roughness, which was previously found to be beneficial for osteoblast adhesion and viability.[9] The bright-field TEM micrographs of the Ag/Ca-P(2) coating in Figure 4b,c reveals the nanoplates of Ca-P and the attachment of silver nanoparticles with uniform distribution on the Ca-P plates without any agglomeration. The homogeneous distribution of the silver nanoparticles is a critical parameter in determining the successful application of the nanoparticles.[40]
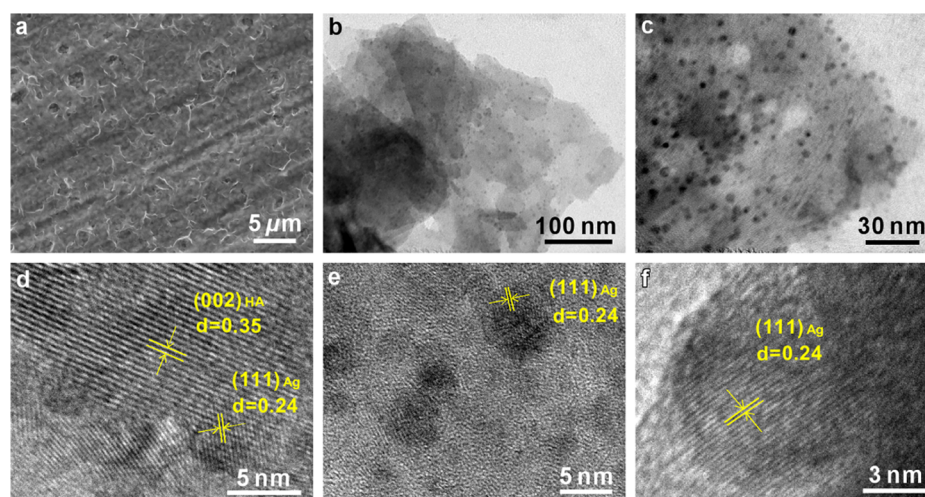
Figure 4. (a) SEM micrograph, (b−c) TEM micrographs and (d−f) HRTEM micrographs of the Ag/Ca-P(2) coating.

The EDS spectra confirm that the attached particles are silver, which is in agreement with the XRD results. The Ag/Ca-P(2) coating is further investigated using high-resolution TEM (HRTEM) (Figure 4d−f). Figure 4d displays the lattice fringes of both Ca-P plates and silver nanoparticles. The interplanar spacing is estimated to be 0.35 and 0.24 nm for the Ca-P and silver, respectively, which is identified as (002) planes of HA and (111) planes of silver ($d_{002,HA}$ = 0.344 nm and $d_{111,Ag}$ = 0.236 nm). According to the TEM and HRTEM observations, the diameter of the silver nanoparticles ranges between 3 and 7 nm. In summary, during the deposition of the Ag/Ca-P(2) coating in the second step, through the cathodic reaction, the silver ions reduce to metallic silver and deposit as silver nanoparticles on the Ca-P coating.

3.2. Silver Release of Ag/Ca-P Coatings. Figure 5 shows the silver ions release profile from Ag/Ca-P coatings as a
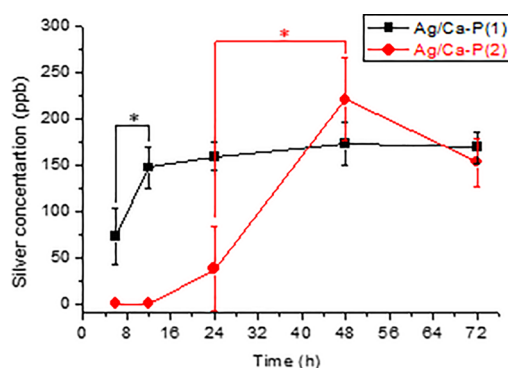

Figure 5. Silver ions release profile from Ag/Ca-P coatings as a function of time in PBS solution. *$p \leq 0.05$.

function of time in PBS solution. Initially, a fast release of Ag^+ appears from the Ag/Ca-P(1) coating in the first 12 h of immersion, which can prevent the initial bacterial adhesion and biofilm formation.[41] After 12 h, the Ag^+ release rate from Ag/Ca-P(1) coating gradually slows down and reaches a near steady-state with the maximum released silver of 173.5 ± 23 ppb. The amount of released silver in PBS from the Ag/Ca-P(1) coating is determined to be more than the amount released from the Ag/Ca-P(2) coating before 48 h. For the Ag/Ca-P(2) coating, the silver release is not detected at the

first 12 h, and after 24 h only 37.3 ± 45 ppb silver ions are released. The maximum concentration of the silver released from the Ag/Ca-P(2) coating is 220.7 ± 45 ppb after 48 h. The difference in the releasing behavior of the silver from the Ag/Ca-P coatings can be explained by the differences in the silver species.[42] The Ag/Ca-P(1) coating contains microsized silver phosphate particles, whereas silver is deposited on the Ag/Ca-P(2) coating as silver nanoparticles. The dissolution rate of a silver component in aqueous solutions is higher than that of metallic silver,[43] resulting in different silver release rates from the two Ag/Ca-P coatings.

3.3. Antimicrobial Evaluation of Ag/Ca-P Coatings. The antimicrobial mechanism can be due to one of the following reasons: (1) direct contact with antimicrobial material (in this case Ag_3PO_4 or AgNPs) and (2) interaction with silver ions released from antimicrobial material. Since the silver release rate of the Ag/Ca-P coatings is a function of time, to evaluate the antimicrobial properties of the Ag/Ca-P coatings, a series of experiments are designed as pretreatments prior to bacteria incubation and the antimicrobial properties are evaluated via colony count method and live/dead staining test. The pretreatments include the immersion of the coatings inside PBS, ultrapure water, and culture medium for 48 h. S. aureus with the initial concentration of 1.0×10^5 CFU/mL are added on the coatings either directly or after the pretreatment. The results are shown as a bacterial reduction percentage compared to control (Figure 6a) and the number of CFUs (Figure 6b). As shown in Figure 6a, when the bacteria are directly added on the coatings, without any pretreatment, the number of S. aureus decreases by 76.1 ± 8.3 and 83.7 ± 4.5% for Ag/Ca-P(1) and Ag/Ca-P(2) coatings, respectively. The antimicrobial activity improves to 97.6 ± 2 and 99.7 ± 0.4% for the Ag/Ca-P(1) and Ag/Ca-P(2) coatings, respectively, which have been pretreated in PBS solution for 48 h. Pretreating the coatings in ultrapure water does not change the bacteria reduction percentage compared to the coatings without the pretreatment. However, immersing the coatings in the culture medium significantly suppresses the antimicrobial activity, which may be due to sedimentation of proteins existing in the culture medium and thereby covering the surface of the coatings. The differences in coating effectiveness due to the different treatments indicate that the effectiveness may be drastically enhanced or suppressed by the experimental
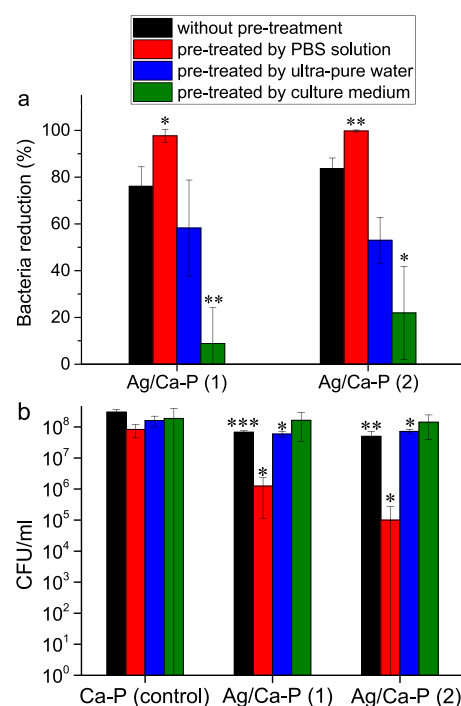
Figure 6. (a) Percentage of bacteria reduction against *S. aureus* and (b) number of CFUs after 24 h incubation on the Ca-P and Ag/Ca-P coatings with and without the pretreatment in different media. $*p \leq 0.05$, $**p \leq 0.005$, and $***p \leq 0.001$.

setup and it emphasizes that all factors carefully need to be taken into account. Figure 6b illustrates that the number of CFUs on the Ag/Ca-P coatings is significantly lower than that of on the Ca-P coating as the control for all groups of the coatings except the coatings treated in the culture medium. Considering the planktonic bacteria, almost the same trend is observed for the bacterial reduction percentage and the number of CFUs (see Figure SI1 in the Supporting Information). In conclusion, although the coatings without any pretreatment possess outstanding antimicrobial activities, the pretreatment in PBS for 48 h remarkably improves the

antimicrobial activity of the coatings, which is a procedure that is easily implemented into clinical settings and enhances the usability and clinical effectiveness of the coating.

Representative fluorescence micrographs of *S. aureus* on the Ca-P and Ag/Ca-P coatings without any pretreatment and coatings pretreated by PBS are shown in Figure 7. Figure 7b1,b2 indicates that there is a minimal number of alive bacteria in the first 6 h of incubation on the Ag/Ca-P(1) coating without the pretreatment. The absence of dead bacteria on the Ag/Ca-P(1) coating in the first 6 h of incubation can be attributed to the high release rate of silver ions from Ag_3PO_4 particles (Figure 5), which prevents bacteria to adhere to the surface of the coating.[41] During the deposition of the Ca-P coatings, one-third of the titanium substrate is not coated because of the deposition setup. This area acts as an internal control to elucidate potential killing mechanisms. Interestingly, the number of alive bacteria in the noncoated titanium section where the rest contains the Ag/Ca-P(1) coating, is minimal (see Figures SI2 and SI3 in the Supporting Information). Based on these results, it can be concluded that the antimicrobial mechanism of Ag/Ca-P(1) coating at the first 6 h of incubation is leaching killing as it also affects the noncoated area drastically. However, after 24 h of incubation (Figure 7b3), both live and dead bacteria are visible on the coating surface. Nevertheless, the validity of bacteria growing on the Ag/Ca-P(1) coating is much lower than that on the control coating (Figure 7a3), which is in agreement with CFU counting results in Figure 6. It seems that the Ag/Ca-P(1) coating loses its antimicrobial activity to some degree after 24 h of incubation, which is attributed to the crystallographic structure of Ag_3PO_4 particles. Yeo et al.[30] reported that in the first 8 h of incubation, both cubic and rhombic dodecahedral Ag_3PO_4 have excellent antimicrobial activity. However, after 10 h of incubation, *E. coli* can grow in the presence of rhombic dodecahedral Ag_3PO_4. The number of silver ions on the {100} surfaces of cubic Ag_3PO_4 is much higher than that on the {110} surfaces of rhombic dodecahedral Ag_3PO_4. As a result, the increased number of live bacteria after 24 h of incubation is attributed to the structure of the deposited rhombic dodecahedral Ag_3PO_4 crystals in the Ag/Ca-P(1) coating. In
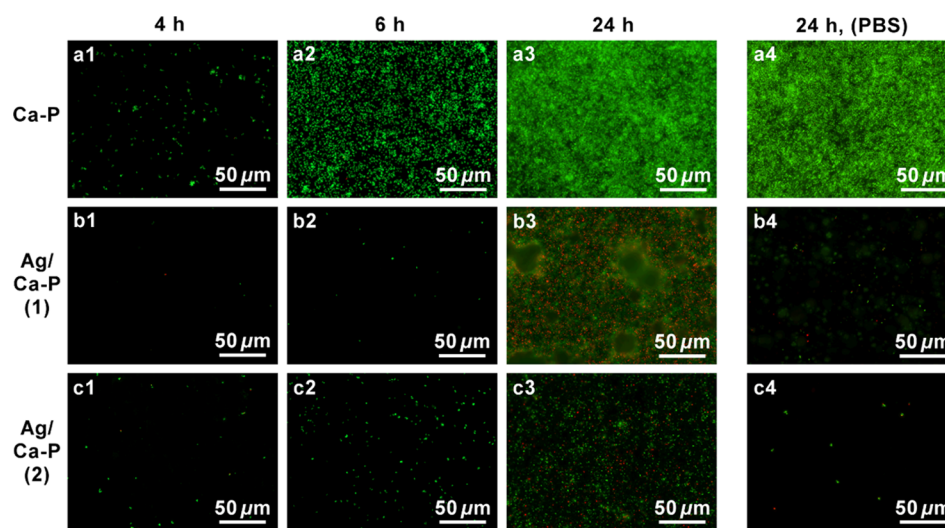

Figure 7. Fluorescence microscopy images of *S. aureus* on (a) Ca-P coating as control, (b) Ag/Ca-P(1) coating, and (c) Ag/Ca-P(2) coating after incubation for (a1−c1) 4 h, (a2−c2) 6 h and (a3−c3) 24 h, and (a4−c4) after 24 h incubation on the coatings pretreated by PBS solution. Green and red indicate live and dead bacteria, respectively.
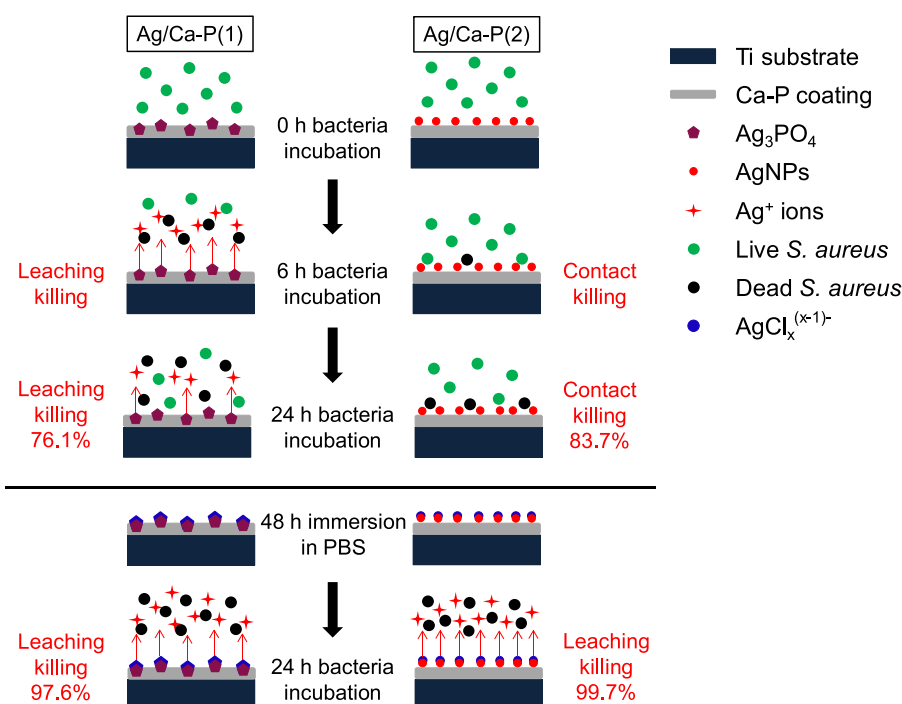
Figure 8. Schematic illustration of the killing mechanism of Ag/Ca-P coatings.

the case of nontreated Ag/Ca-P(2) coating, the fluorescence microscopy images (Figure 7c1−c3) illustrate that, at all the time points, the number of live bacteria on the coating is much lower than that on the control. Additionally, the absence of dead bacteria at the first 6 h of incubation on the Ag/Ca-P(2) coating suggests that AgNPs mainly prevent bacterial growth through physical contact. According to the ICP results, by the first 12 h, silver ion release from the Ag/Ca-P(2) coating is minimal. Therefore, the main antimicrobial mechanism of the Ag/Ca-P(2) coating is contact killing.[25,26] The considerable amount of alive bacteria on the noncoated titanium section of the Ag/Ca-P(2) coating after 6 h of incubation (see Figure SI3 in the Supporting Information) also supports the contact killing mechanism. After 24 h of incubation, the number of alive bacteria on the Ag/Ca-P(2) coating increases but still is much lower than on the control coating. Figure 7a4−c4 shows the bacteria cultured for 24 h on the coatings pretreated by PBS. On the Ca-P coating, a significant number of live bacteria adhere and form a dense biofilm. In contrast, on the Ag/Ca-P(1) and Ag/Ca-P(2) coatings, only a small number of alive bacteria are observed. Besides, there are just a few alive bacteria on the noncoated titanium section of these coatings (see Figure SI2 in the Supporting Information). In conclusion, the antimicrobial mechanism of both the Ag/Ca-P(1) and Ag/Ca-P(2) coatings pretreated by PBS is leaching killing. The results of live/dead staining confirm the impressive bacterial reduction on the pretreated Ag/Ca-P coatings concluded from CFU counting.

The improvement of antimicrobial activity through immersing the Ag/Ca-P coatings inside PBS is associated with the presence of chloride ions in the PBS solution. In general, the presence of chloride ions influences the toxicity of silver species due to the formation of solid AgCl, which has a very low solubility (K_{sp} = 1.77 × 10^{-10} mol/L^2).[44,45] However, in higher concentration of chloride, there is a possibility of formation of soluble AgCl$_x^{(x−1)−}$ species, resulting in enhanced antimicrobial activity.[46] Levard et al.[47] studied the stability and dissolution kinetics of AgNPs in the presence of chloride ions and also its effect on the growth inhibition of *E. coli*. They reported that a low amount of chloride ions in the solution remarkably decreases the release rate of AgNPs due to the precipitation of solid AgCl. Nevertheless, by increasing the concentration of chloride ions, the solid AgCl becomes thermodynamically unstable, and the dominant phase would be soluble AgCl$_x^{(x−1)−}$ species, resulting in higher dissolution rate of AgNPs compared to that in deionized (DI) water control. They also claimed that the toxicity of AgNPs toward *E. coli* is due to the soluble species of Ag rather than the AgNP effect. Consequently, the enhanced antimicrobial activity of the pretreated Ag/Ca-P coatings is attributed to the formation of AgCl$_x^{(x−1)−}$ species and the presence of the chloride in the Ag/Ca-P coatings is proved by EDS analysis (see Figure SI4 in the Supporting Information). These results also coincide with the release study of silver ions in PBS where after 24 h the release increases indicating that this time is needed to form a suitable amount of AgCl$_x^{(x−1)−}$ species to become detectable and active towards bacteria. Similar results were obtained by heat treatment of Ag/Ca-P coatings. Zhang et al.[48] reported improvement of the antimicrobial activity of Ag/Ca-P coatings through heat treatment. They found that heat treatment in air results in silver oxide formation, which is more susceptible to leaching silver ions than the unheated silver nanoparticles. However, considering the simplicity of the PBS treatment, immersion inside the PBS solution is more preferable to enhance the antimicrobial activity of the coatings.

A schematic illustration of the proposed antimicrobial mechanism of the Ag/Ca-P coatings is shown in Figure 8. In the case of Ag/Ca-P(1) coating, the high release rate of silver ions from Ag$_3$PO$_4$ in the first 6 h of bacteria incubation results in leaching killing. After 24 h bacteria incubation, the silver release rate slowly decreases, but still the antimicrobial mechanism is leaching killing, and the bacteria reduction is

76.1 ± 8.3%. In contrast, in the case of Ag/Ca-P(2) coating, the antimicrobial mechanism is mainly contact killing due to the very low amount of silver release even after 24 h of incubation, and the bacteria reduction is 83.7 ± 4.5%. However, if the Ag/Ca-P coatings are pretreated by PBS, due to the high concentration of chloride ions in PBS, soluble $AgCl_x^{(x-1)-}$ species will form on both Ag_3PO_4 and AgNPs. When the pretreated coatings are exposed to bacteria solution, the high release rate of silver ions from soluble $AgCl_x^{(x-1)-}$ species causes bacterial reduction of 97.6 ± 2.7 and 99.7 ± 0.4% for Ag/Ca-P(1) and Ag/Ca-P(2) coating, respectively, which is associated to the leaching killing.

3.4. SaOs Osteoblast Cell Response on Ag/Ca-P Coatings.

A successfully modified surface should fulfill not only the antimicrobial activity against bacteria but also the cytocompatibility toward the mammalian cells. To evaluate the biocompatibility of Ag/Ca-P coatings, SaOs cells are cultured for 24 h on the coatings and their behavior is investigated via XTT assay, live/dead cell staining test, and SEM observation. Figure 9 shows the metabolic activity and the number of living
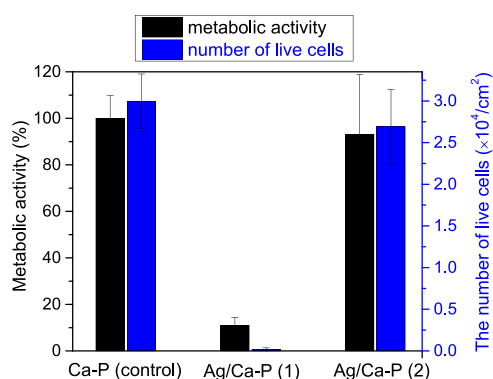

Figure 9. Metabolic activity (XTT assay) and the number of live SaOs cells after 24 h incubation on the coatings.

cells per unit surface area on the Ag/Ca-P coatings, as well as on the Ca-P coating as the control. The metabolic activity of the cells on the Ag/Ca-P(1) coating is very low, suggesting that the Ag/Ca-P(1) coating is cytotoxic for SaOs cells.[49] Nevertheless, the metabolic activity of cells on the Ag/Ca-P(2) coating and the control is very similar. Likewise, the number of

live cells on Ag/Ca-P(1) coating is almost zero. However, the number of live cells on the Ag/Ca-P(2) and the Ca-P coatings are comparable and no significant difference is observed, which is in agreement with the XTT assay results and indicates that Ag/Ca-P(2) coating is biocompatible while the Ag/Ca-P(1) coating is not.

Figure 10 shows the fluorescence microscopy and SEM images of SaOs cells cultured for 24 h on the Ca-P and Ag/Ca-P(2) coatings. As shown in the fluorescence images, almost all of the cells are alive on the control and the Ag/Ca-P(2) coating (Figure 10a1,b1). Furthermore, the SEM images illustrate that the SaOs cells spread out and attach very well on the coatings with abundant lamellipodia and filopodia extensions. The SEM images of an individual cell (Figure 10a3,b3) reveal that the morphology of the cell on the Ag/Ca-P(2) coating is comparable with those on the control. These findings indicate that the presence of AgNPs in the Ag/Ca-P(2) coating does not influence the viability and morphology of the SaOs cell and the coating is biocompatible. Earlier studies also have reported that the surfaces, which were decorated by AgNPs have excellent antimicrobial properties meanwhile could support the viability of mammalian cells without cytotoxicity.[19,24,50]

The development of a functional biomedical implant includes surface modifications that can accomplish a good interaction with the human body in terms of biocompatibility and bioactivity, along with the prevention of implant-associated infections. The calcium phosphate coatings containing silver nanoparticles (Ag/Ca-P(2)) possess all these properties, therefore are promising candidates for modifying biomedical implants. Our findings have important indications in evaluating the role of silver type in the antimicrobial properties and biocompatibility of silver-containing calcium phosphate coatings.

4. CONCLUSIONS

The physicochemical characteristics of silver in the silver-containing coatings are crucial factors influencing antimicrobial activity and cytotoxicity of the coatings. In this research, silver-containing calcium phosphate coatings are deposited on titanium substrates via electrochemical deposition to study their antimicrobial properties and biocompatibility regarding the silver type inside the coatings. Silver in the Ag/Ca-P(1)
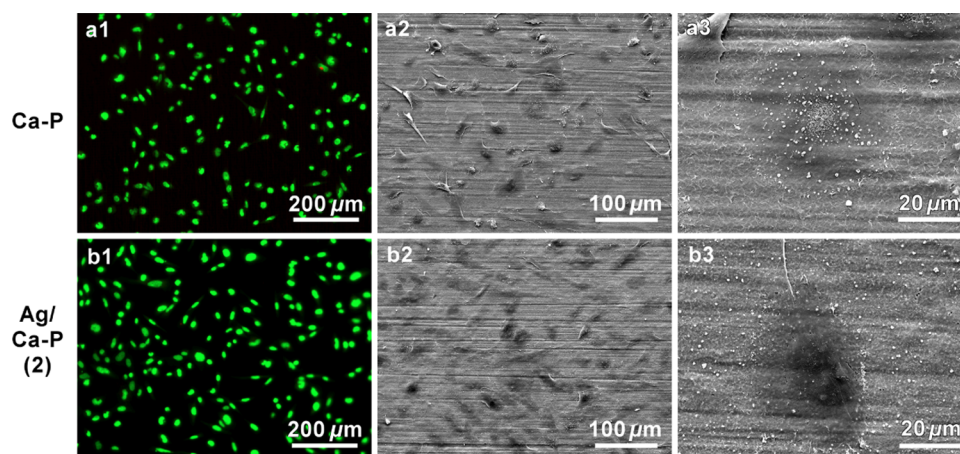

Figure 10. (a1, b1) Fluorescence microscopy and (a2−a3, b2−b3) scanning electron microscopy images of *S. aureus* after incubation for 24 h on (a) Ca-P coating as control, (b) Ag/Ca-P(2) coating. Green and red indicate live and dead bacteria, respectively.

coating has the ionic chemical state, and deposits as microsized silver phosphate particles embedded inside the Ca-P matrix. Whereas, in the Ag/Ca-P(2) coating, silver deposits as metallic nanoparticles on the Ca-P coating. The antimicrobial evaluation against *S. aureus* reveals that the high release rate of silver ions from the Ag/Ca-P(1) coating results in leaching killing, and the bacteria reduction is 76.1 ± 8.3%. The antimicrobial mechanism of the Ag/Ca-P(2) coating is mainly contact killing, and the bacteria reduction is 83.7 ± 4.5%. Pretreatment by PBS leads to improvement of the bacteria reduction to 97.6 ± 2.7 and 99.7 ± 0.4% for Ag/Ca-P(1) and Ag/Ca-P(2) coating, respectively. The enhanced antimicrobial activity after PBS treatment can be attributed to the formation of soluble $AgCl_x^{(x-1)-}$ species on the Ag_3PO_4 and AgNPs, which results in a high silver release rate and leaching killing. According to the biocompatibility assay, the Ag/Ca-P(1) coating is cytotoxic towards the cells. In contrast, the Ag/Ca-P(2) coating shows excellent biocompatibility. The results of the current investigation shows that the electrochemically deposited Ag/Ca-P coatings containing silver nanoparticles with excellent antimicrobial activity accompanied by efficient biocompatibility can be applied to titanium, a commonly used material for medical implants. Although not used here, the electrochemical deposition has the advantage of depositing uniformly on highly irregularly shaped and porous materials. Implants and their design become more complex, also due to the available three-dimensional (3D) printing approaches and hence new strategies for applying highly effective antimicrobial coatings with excellent biocompatibility will accelerate the development and usability of such novel biomedical implants.

■ ASSOCIATED CONTENT

ⓢ Supporting Information

The Supporting Information is available free of charge at https://pubs.acs.org/doi/10.1021/acsami.9b20158.

> Planktonic bacteria reduction on the Ag/Ca-P coatings; An image of coated Ti disc; fluorescence microscopy images of *S. aureus* on noncoated Ti section of the samples; EDS analysis of the Ag/Ca-P(2) coating after pretreatment (PDF)

■ AUTHOR INFORMATION

Corresponding Author

P. van Rijn — *University of Groningen, Groningen, The Netherlands;* ⓞ orcid.org/0000-0002-2208-5725; Email: p.van.rijn@umcg.nl

Other Authors

T. Mokabber — *University of Groningen, Groningen, The Netherlands*

H. T. Cao — *University of Groningen, Groningen, The Netherlands*

N. Norouzi — *University of Groningen, Groningen, The Netherlands*

Y. T. Pei — *University of Groningen, Groningen, The Netherlands;* ⓞ orcid.org/0000-0002-1817-2228

Complete contact information is available at: https://pubs.acs.org/10.1021/acsami.9b20158

■ REFERENCES

(1) Monsees, T. K. Biocompatibility and Anti-Microbiological Activity Characterization of Novel Coatings for Dental Implants: A Primer for Non-Biologists. *Front. Mater.* **2016**, *3*, No. 40.

(2) Campoccia, D.; Montanaro, L.; Arciola, C. R. A Review of the Biomaterials Technologies for Infection-Resistant Surfaces. *Biomaterials* **2013**, *34*, 8533−8554.

(3) Zhou, Q.; Ge, L.; Guimaraes, C. F.; Kuhn, P. T.; Yang, L.; van Rijn, P. Development of a Novel Orthogonal Double Gradient for High-Throughput Screening of Mesenchymal Stem Cells-Materials Interaction. *Adv. Mater. Interfaces* **2018**, *5*, No. 1800504.

(4) Swartjes, J. J. T. M.; Sharma, P. K.; van Kooten, T. G.; van der Mei, H. C.; Mahmoudi, M.; Busscher, H. J.; Rochford, E. T. J. Current Developments in Antimicrobial Surface Coatings for Biomedical Applications. *Curr. Med. Chem.* **2015**, *22*, 2116−2129.

(5) Neut, D.; Dijkstra, R. J. B.; Thompson, J. I.; Kavanagh, C.; van der Mei, H. C.; Busscher, H. J. A Biodegradable Gentamicin-Hydroxyapatite-Coating for Infection Prophylaxis in Cementless Hip Prostheses. *Eur. Cells Mater.* **2015**, *29*, 42−56.

(6) Spriano, S.; Yamaguchi, S.; Baino, F.; Ferraris, S. A Critical Review of Multifunctional Titanium Surfaces: New Frontiers for Improving Osseointegration and Host Response, Avoiding Bacteria Contamination. *Acta Biomater.* **2018**, *79*, 1−22.

(7) Keskin, D.; Mergel, O.; van der Mei, H. C.; Busscher, H. J.; van Rijn, P. Inhibiting Bacterial Adhesion by Mechanically Modulated Microgel Coatings. *Biomacromolecules* **2019**, *20*, 243−253.

(8) Zhao, B.; van der Mei, H. C.; Subbiahdoss, G.; de Vries, J.; Rustema-Abbing, M.; Kuijer, R.; Busscher, H. J.; Ren, Y. Soft Tissue Integration versus Early Biofilm Formation on Different Dental Implant Materials. *Dent. Mater.* **2014**, *30*, 716−727.

(9) Mokabber, T.; Zhou, Q.; Vakis, A. I.; van Rijn, P.; Pei, Y. T. Mechanical and Biological Properties of Electrodeposited Calcium Phosphate Coatings. *Mater. Sci. Eng., C* **2019**, *100*, 475−484.

(10) Costerton, J. W.; Montanaro, L.; Arciola, C. R. Biofilm in Implant Infections: Its Production and Regulation. *Int. J. Artif. Organs* **2005**, *28*, 1062−1068.

(11) Hall-Stoodley, L.; Costerton, J. W.; Stoodley, P. Bacterial Biofilms: From the Natural Environment to Infectious Diseases. *Nat. Rev. Microbiol.* **2004**, *2*, 95−108.

(12) Mocanu, A.; Furtos, G.; Rapuntean, S.; Horovitz, O.; Flore, C.; Garbo, C.; Danisteanu, A.; Rapuntean, G.; Prejmerean, C.; Tomoaia-Cotisel, M. Synthesis; Characterization and Antimicrobial Effects of Composites Based on Multi-Substituted Hydroxyapatite and Silver Nanoparticles. *Appl. Surf. Sci.* **2014**, *298*, 225−235.

(13) van de Belt, H.; Neut, D.; Schenk, W.; van Horn, J. R.; van der Mei, H. C.; Busscher, H. J. Infection of Orthopedic Implants and the Use of Antibiotic-Loaded Bone Cements. A Review. *Acta Orthop. Scand.* **2001**, *72*, 557−571.

(14) Chen, Y.; Zheng, X.; Xie, Y.; Ji, H.; Ding, C.; Li, H.; Dai, K. Silver Release from Silver-Containing Hydroxyapatite Coatings. *Surf. Coat. Technol.* **2010**, *205*, 1892−1896.

(15) Zhao, L.; Chu, P. K.; Zhang, Y.; Wu, Z. Antibacterial Coatings on Titanium Implants. *J. Biomed. Mater. Res., Part B* **2009**, *91B*, 470−480.

(16) Chouirfa, H.; Bouloussa, H.; Migonney, V.; Falentin-Daudré, C. Review of Titanium Surface Modification Techniques and Coatings for Antibacterial Applications. *Acta Biomater.* **2019**, *83*, 37−54.

(17) Shi, C.; Gao, J.; Wang, M.; Shao, Y.; Wang, L.; Wang, D.; Zhu, Y. Functional Hydroxyapatite Bioceramics with Excellent Osteoconductivity and Stern-Interface Induced Antibacterial Ability. *Biomater. Sci.* **2016**, *4*, 699−710.

(18) Roy, M.; Fielding, G. A.; Beyenal, H.; Bandyopadhyay, A.; Bose, S. Mechanical, in Vitro Antimicrobial, and Biological Properties of Plasma-Sprayed Silver-Doped Hydroxyapatite Coating. *ACS Appl. Mater. Interfaces* **2012**, *4*, 1341−1349.

(19) Xie, C. M.; Lu, X.; Wang, K. F.; Meng, F. Z.; Jiang, O.; Zhang, H. P.; Zhi, W.; Fang, L. M. Silver Nanoparticles and Growth Factors Incorporated Hydroxyapatite Coatings on Metallic Implant Surfaces for Enhancement of Osteoinductivity and Antibacterial Properties. *ACS Appl. Mater. Interfaces* **2014**, *6*, 8580−8589.

(20) Ke, D.; Vu, A. A.; Bandyopadhyay, A.; Bose, S. Compositionally Graded Doped Hydroxyapatite Coating on Titanium Using Laser and Plasma Spray Deposition for Bone Implants. *Acta Biomater.* **2019**, *84*, 414−423.

(21) Cai, S.; Pourdeyhimi, B.; Loboa, E. G. Industrial-Scale Fabrication of an Osteogenic and Antibacterial PLA/Silver-Loaded Calcium Phosphate Composite with Significantly Reduced Cytotoxicity. *J. Biomed. Mater. Res., Part B* **2019**, *107*, 900−910.

(22) Le Ouay, B.; Stellacci, F. Antibacterial Activity of Silver Nanoparticles: A Surface Science Insight. *Nano Today* **2015**, *10*, 339−354.

(23) Sahni, G.; Gopinath, P.; Jeevanandam, P. A Novel Thermal Decomposition Approach to Synthesize Hydroxyapatite-Silver Nanocomposites and Their Antibacterial Action against GFP-Expressing Antibiotic Resistant *E. coli. Colloids Surf., B* **2013**, *103*, 441−447.

(24) Cao, H.; Qiao, Y.; Liu, X.; Lu, T.; Cui, T.; Meng, F.; Chu, P. K. Electron Storage Mediated Dark Antibacterial Action of Bound Silver Nanoparticles: Smaller Is Not Always Better. *Acta Biomater.* **2013**, *9*, 5100−5110.

(25) Orozco Carmona, V.; Martinez Perez, C.; de Lima, R.; Fernandes Fraceto, L.; Romero Garcia, J.; Ledezma Perez, A.; Marke, S.; Rodriguez Gonzalez, C.; Hurtado Macias, A.; Martinez-Villafane, A. Effect of Silver Nanoparticles in a Hydroxyapatite Coating Applied by Atmospheric Plasma Spray. *Int. J. Electrochem. Sci.* **2014**, *9*, 7471−7494.

(26) Cao, H.; Liu, X.; Meng, F.; Chu, P. K. Biological Actions of Silver Nanoparticles Embedded in Titanium Controlled by Micro-Galvanic Effects. *Biomaterials* **2011**, *32*, 693−705.

(27) Shirkhanzadeh, M. Direct Formation of Nanophase Hydroxyapatite on Cathodically Polarized Electrodes. *J. Mater. Sci. Mater. Med.* **1998**, *9*, 67−72.

(28) Fu, C.; Zhang, X.; Savino, K.; Gabrys, P.; Gao, Y.; Chaimayo, W.; Miller, B. L.; Yates, M. Z. Antimicrobial Silver-Hydroxyapatite Composite Coatings through Two-Stage Electrochemical Synthesis. *Surf. Coat. Technol.* **2016**, *301*, 13−19.

(29) Mokabber, T.; Lu, L. Q.; van Rijn, P.; Vakis, A. I.; Pei, Y. T. Crystal Growth Mechanism of Calcium Phosphate Coatings on Titanium by Electrochemical Deposition. *Surf. Coat. Technol.* **2018**, *334*, 526−535.

(30) Yeo, B. E.; Seo, Y.; Park, H.; Huh, Y. D. Facet Effect of Ag3PO4 Crystals on Antibacterial Activities. *Bull. Korean Chem. Soc.* **2015**, *36*, 1904−1907.

(31) Chen, X.; Dai, Y.; Wang, X. Methods and Mechanism for Improvement of Photocatalytic Activity and Stability of Ag3PO4: A Review. *J. Alloys Compd.* **2015**, *649*, 910−932.

(32) Xu, Y.-S.; Zhang, W.-D. Morphology-Controlled Synthesis of Ag3PO4 Microcrystals for High Performance Photocatalysis. *CrystEngComm* **2013**, *15*, 5407−5411.

(33) Godoy-Gallardo, M.; Rodríguez-Hernández, A. G.; Delgado, L. M.; Manero, J. M.; Javier Gil, F.; Rodríguez, D. Silver Deposition on Titanium Surface by Electrochemical Anodizing Process Reduces Bacterial Adhesion of Streptococcus Sanguinis and Lactobacillus Salivarius. *Clin. Oral Implants Res.* **2015**, *26*, 1170−1179.

(34) Ciobanu, C. S.; Iconaru, S. L.; Pasuk, I.; Vasile, B. S.; Lupu, A. R.; Hermenean, A.; Dinischiotu, A.; Predoi, D. Structural Properties of Silver Doped Hydroxyapatite and Their Biocompatibility. *Mater. Sci. Eng., C* **2013**, *33*, 1395−1402.

(35) Li, M.; Liu, Q.; Jia, Z.; Xu, X.; Shi, Y.; Cheng, Y.; Zheng, Y. Polydopamine-Induced Nanocomposite Ag/CaP Coatings on the Surface of Titania Nanotubes for Antibacterial and Osteointegration Functions. *J. Mater. Chem. B* **2015**, *3*, 8796−8805.

(36) Akhavan, O.; Ghaderi, E. Self-Accumulated Ag Nanoparticles on Mesoporous TiO2 Thin Film with High Bactericidal Activities. *Surf. Coat. Technol.* **2010**, *204*, 3676−3683.

(37) Huang, Y.; Wang, W.; Zhang, X.; Liu, X.; Xu, Z.; Han, S.; Su, Z.; Liu, H.; Gao, Y.; Yang, H. A Prospective Material for Orthopedic Applications: Ti Substrates Coated with a Composite Coating of a Titania-Nanotubes Layer and a Silver-Manganese-Doped Hydroxyapatite Layer. *Ceram. Int.* **2018**, *44*, 5528−5542.

(38) Rameshbabu, N.; Kumar, T. S. S.; Prabhakar, T. G.; Sastry, V. S.; Murty, K. V. G. K.; Rao, K. P. Antibacterial Nanosized Silver Substituted Hydroxyapatite: Synthesis and Characterization. *J. Biomed. Mater. Res., Part A* **2007**, *80A*, 581−591.

(39) Sygnatowicz, M.; Keyshar, K.; Tiwari, A. Antimicrobial Properties of Silver-Doped Hydroxyapatite Nano-Powders and Thin Films. *JOM* **2010**, *62*, 65−70.

(40) Agnihotri, S.; Mukherji, S.; Mukherji, S. Immobilized Silver Nanoparticles Enhance Contact Killing and Show Highest Efficacy: Elucidation of the Mechanism of Bactericidal Action of Silver. *Nanoscale* **2013**, *5*, 7328−7340.

(41) Honda, M.; Kawanobe, Y.; Ishii, K.; Konishi, T.; Mizumoto, M.; Kanzawa, N.; Matsumoto, M.; Aizawa, M. In Vitro and in Vivo Antimicrobial Properties of Silver-Containing Hydroxyapatite Prepared via Ultrasonic Spray Pyrolysis Route. *Mater. Sci. Eng., C* **2013**, *33*, 5008−5018.

(42) Noda, I.; Miyaji, F.; Ando, Y.; Miyamoto, H.; Shimazaki, T.; Yonekura, Y.; Miyazaki, M.; Mawatari, M.; Hotokebuchi, T. Development of Novel Thermal Sprayed Antibacterial Coating and Evaluation of Release Properties of Silver Ions. *J. Biomed. Mater. Res., Part B* **2009**, *89B*, 456−465.

(43) Dubnika, A.; Loca, D.; Salma, I.; Reinis, A.; Poca, L.; Berzina-Cimdina, L. Evaluation of the Physical and Antimicrobial Properties of Silver Doped Hydroxyapatite Depending on the Preparation Method. *J. Mater. Sci.: Mater. Med.* **2014**, *25*, 435−444.

(44) Gokcekaya, O.; Ueda, K.; Ogasawara, K.; Narushima, T. Antibacterial Activity of Ag Nanoparticle-Containing Hydroxyapatite Powders in Simulated Body Fluids with Cl Ions. *Mater. Chem. Phys.* **2019**, *223*, 473−478.

(45) Li, X.; Lenhart, J. J.; Walker, H. W. Dissolution-Accompanied Aggregation Kinetics of Silver Nanoparticles. *Langmuir* **2010**, *26*, 16690−16698.

(46) Gupta, A.; Maynes, M.; Silver, S. Effects of Halides on Plasmid-Mediated Silver Resistance in *Escherichia coli. Appl. Environ. Microbiol.* **1998**, *64*, 5042−5045.

(47) Levard, C.; Mitra, S.; Yang, T.; Jew, A. D.; Badireddy, A. R.; Lowry, G. V.; Brown, G. E. Effect of Chloride on the Dissolution Rate of Silver Nanoparticles and Toxicity to *E. coli. Environ. Sci. Technol.* **2013**, *47*, 5738−5745.

(48) Zhang, X.; Chaimayo, W.; Yang, C.; Yao, J.; Miller, B. L.; Yates, M. Z. Silver-Hydroxyapatite Composite Coatings with Enhanced Antimicrobial Activities through Heat Treatment. *Surf. Coat. Technol.* **2017**, *325*, 39−45.

(49) Furko, M.; Bella, E. D.; Fini, M.; Balázsi, C. Corrosion and Biocompatibility Examination of Multi-Element Modified Calcium Phosphate Bioceramic Layers. *Mater. Sci. Eng., C* **2019**, *95*, 381−388.

(50) Herkendell, K.; Shukla, V. R.; Patel, A. K.; Balani, K. Domination of Volumetric Toughening by Silver Nanoparticles over Interfacial Strengthening of Carbon Nanotubes in Bactericidal Hydroxyapatite Biocomposite. *Mater. Sci. Eng., C* **2014**, *34*, 455−467.

■ NOTE ADDED AFTER ASAP PUBLICATION

Due to a production error, this paper was published on the Web on January 14, 2020, with errors on the y-axis of Figure 5. The corrected version was reposted on January 21, 2020.